International Journal of Solids and Structures 50 (2013) 1710–1720

Contents lists available at SciVerse ScienceDirect

International Journal of Solids and Structures

journal homepage: www.elsevier.com/locate/ijsolstr

The Proper Generalized Decomposition (PGD) as a numerical procedure to solve 3D cracked plates in linear elastic fracture mechanics

Eugenio Giner [a,*], Brice Bognet [b], Juan J. Ródenas [a], Adrien Leygue [b], F. Javier Fuenmayor [a], Francisco Chinesta [b]

[a] Centro de Investigación de Tecnología de Vehículos – CITV, Depto. de Ingeniería Mecánica y de Materiales, Universitat Politècnica de València, Camino de Vera, 46022 Valencia, Spain
[b] EADS Corporate Foundation International Chair GeM – Ecole Centrale de Nantes, 1 rue de la Noe, BP 92101, F-44321 Nantes cedex 3, France

ARTICLE INFO

Article history:
Received 8 August 2012
Received in revised form 31 December 2012
Available online 13 February 2013

Keywords:
Proper Generalized Decomposition
Finite element method
Cracked plate
Corner singularity

ABSTRACT

In this work, we present a new approach to solve linear elastic crack problems in plates using the so-called Proper Generalized Decomposition (PGD). In contrast to the standard FE method, the method enables to solve the crack problem in an efficient way by obtaining a single solution in which the Poisson's ratio ν and the plate thickness B are non-fixed parameters. This permits to analyze the influence of ν and B in the 3D solutions at roughly the cost of a series expansion of 2D analyses. Computationally, the PGD solution is less expensive than a full 3D standard FE analysis for typical discretizations used in practice to capture singularities in 3D crack problems. In order to verify the effectiveness of the proposed approach, the method is applied to cracked plates in mode I with a straight-through crack and a quarter-elliptical corner crack, validating J-integral results with different reference solutions.

1. Introduction

The elastic analysis of three dimensional cracks in plates has been extensively considered in the fracture mechanics literature. Early analytical approaches for 3D crack problems were provided by the pioneering works of Hartranft and Sih (1969), Hartranft and Sih (1970), Sih (1971), Benthem (1977) and Bažant and Estenssoro (1979) and other more recent, such as Zhu (1990) and Leung and Su (1996), etc. As the computational capabilities evolved during the last decades, the analytical studies were soon complemented by an increasing number of numerical works using the finite element method (FEM) (e.g. Newman and Raju, 1983; Nakamura and Parks, 1988; Leung and Su, 1995; Leung and Su, 1996; Kwon and Sun, 2000, etc.). All these studies show that a triaxial stress state arises in the vicinity of the crack front within the body, even for an in-plane loaded cracked plate. As in other stress concentration problems of elasticity, the triaxial stress state is ultimately due to different Poisson contractions that exist within the solid, and therefore the Poisson's ratio ν plays an essential role in the analysis of 3D crack problems.

The existence of the so-called vertex or corner singularity at the intersection of the crack front with the traction-free lateral surfaces is another inherent feature of the 3D crack problem. This phenomenon is accompanied by the loss of stress triaxiality as the traction-free lateral surfaces are approached (loss of constraint). The extent of the influence of the corner singularity and loss of constraint regions have a strong influence on the crack propagation profile and fracture toughness (Bažant and Estenssoro, 1979; Pook, 1994; Pook, 2000; Heyder et al., 2005) and leads to the distinction between the surface and inner regions (Broek, 1986; Anderson, 2005), usually assimilated in a non-rigorous way as two-dimensional plane stress and plane strain states. The extent of these regions depends largely on the a/B ratio (being a the crack length and B the plate thickness). Therefore, the plate thickness B also plays an important role in the analysis of 3D cracked plates.

To the authors' knowledge, no closed-form solution for a 3D crack in a finite thickness plate has been reported to date and many FE studies can be currently found pursuing a better understanding of the 3D crack elastic fields (e.g. Leung and Su (1995), Leung and Su (1996), Kwon and Sun (2000) and Giner et al. (2010)). In this work, we present a new numerical approach to solve cracked plates in an efficient way by obtaining a single solution in which the Poisson's ratio ν and the plate thickness B are non-fixed parameters. To this end, the numerically approximated solution for the displacement field is of the form $\mathbf{u}(x, y, z, \nu, B)$. Using the proposed method, it is possible to obtain a numerical solution for a cracked plate problem with a single analysis that can be particularized for any ν and B by simple post-processing, thus providing an efficient tool for the numerical analysis of these problems. The method makes use of the Proper Generalized Decomposition (PGD), proposed by Chinesta and co-workers (Ammar et al., 2006; Ammar et al., 2007; Bognet et al., 2012) that has recently been applied to many fields of physics and engineering. In this method, the sought

* Corresponding author. Tel.: +34 96 3877621; fax: +34 96 3877629.
E-mail address: eginerm@mcm.upv.es (E. Giner).

0020-7683/$ - see front matter © 2013 Elsevier Ltd. All rights reserved.
http://dx.doi.org/10.1016/j.ijsolstr.2013.01.039

displacement field $\mathbf{u}(x,y,z,\nu,B)$ is written as a series expansion of function products. The formulation proposed here uses a 2D discretization for a given plane times a 1D discretization in the normal direction. In addition, independent functions of ν and B are included in the tentative solution to be converged. An iterative process is then carried out by which the necessary terms of the series expansion are added in order to attain the required accuracy. As a result a 3D problem including two additional coordinates is solved at roughly the cost of a series expansion of 2D analyses. The PGD solution is computationally less expensive than a full 3D standard FE analysis for typical discretizations used in practice to capture singularities in 3D crack problems. From the numerical point of view, this is the first time that the PGD is successfully applied to problems with singularities (both the classical in-plane Williams singularity and the corner singularity).

The essentials of the PGD and the formulation for its application to a fracture problem are given in Section 2. A numerical verification of the results of the method as compared to standard finite element solutions and other reference solutions is provided in Section 3 through the analysis of cracked plate configurations. The results show the usefulness and efficiency of the method, enabling to capture the corner singularity behavior in very good agreement with the results predicted by Benthem (1977) and the numerical solutions provided by Dimitrov et al. (2001). Previously, the analysis of this corner singularity with the standard finite element method has posed difficulties in some works reported in the literature due to its elusive character unless a high degree of refinement is considered. The interested reader can refer to the excellent historical review presented in Kwon and Sun (2000) and the comprehensive work by Schnack et al. (2011). Finally, the method is applied to a quarter-elliptical corner crack in a plate and some results regarding the convergence of the method are presented.

2. Fundamentals of the PGD

2.1. Overview of the method

Proper Generalized Decompositions (PGDs) were proposed recently to alleviate the solution of complex models encountered in science and engineering. The PGD is based on the use of separated representations and, in fact, different kind of separated representations can be envisaged. Ladevèze (1999) proposed in the eighties separating space and time in the solution of non-linear transient thermo-mechanical models within the framework of the LATIN paradigm. Thus, if $u(\mathbf{x},t)$ represents such a solution, it was searched under the separated form:

$$u(\mathbf{x},t) \approx \sum_{i=1}^{n} X_i(\mathbf{x}) \cdot T_i(t) \tag{1}$$

This separated representation was extensively considered in Ladevèze's works, see Ladevèze et al. (2009) and Ladevèze et al. (2010) and the references therein.

We can notice that instead of solving a space problem at each time step, as classically carried out when using standard incremental time integrations, a reduced number of space problems, scaling with n, must be solved for computing the space functions $X_i(\mathbf{x})$ and the same number of one-dimensional problems for computing the time functions $T_i(t)$. Because the computing effort for solving the one-dimensional problems is negligible when compared to the one required for solving a space problem, the computing time savings are impressive when the time step becomes very small.

About twenty years later, the space–time separated representation was generalized for solving efficiently multidimensional models that arise from the fine description of materials within a kinetic theory approach (Ammar et al., 2006; Ammar et al., 2007). Later, it was applied for alleviating the computational complexity when addressing 3D models defined in degenerated domains, in which at least one of its characteristic dimensions is much smaller that the other ones. This is typically the case when calculating 3D solutions of problems defined in plate or shell geometries. In elasticity, when plate and shell theories apply, they allow to reduce the dimensionality from 3D to 2D. However, in some cases fully 3D solutions are preferred due to the existence of either 3D effects close to the plate edges or situations where the Saint–Venant principle fails and consequently 3D effects are present everywhere in the plate. Moreover, in the case of inelastic behavior, the 3D solution is in most of cases mandatory.

In that context, Bognet et al. (2012) proposed an in-plane-out-of-plane separated representation for computing full 3D solutions while keeping a computational cost close to that of 2D solutions. The proposed separated representation of a generic field is then

$$u(x,y,z) \approx \sum_{i=1}^{n} X_i(\mathbf{x}) \cdot Z_i(z) \tag{2}$$

where $\mathbf{x} = (x,y) \in \Omega \subset \mathcal{R}^2$ and $z \in [0,B]$, being B the plate thickness. We note that such a decomposition requires the solution of a number of 2D problems, number that scales with n, for computing functions $X_i(\mathbf{x})$, and the same number of 1D problems involving functions $Z_i(z)$. Thus, even when considering very fine descriptions of functions $Z_i(z)$, the impact in the total computing time remains moderate, in comparison with a fully 3D solution performed using standard discretization techniques. The computational savings are evidenced in Fig. 1, where the computation time of different analyses for a plate problem using the PGD method with a 2D + 1D discretizations is compared to the time of standard 3D FE analyses using 3D solid elements. When the number of degrees of freedom (DOF) in the thickness direction is greater than 10–15, the computational cost of the PGD is less than the standard 3D FEM cost. The difference between both methods increases very rapidly as the number of DOFs of the in-plane and thickness discretizations increases.

Therefore, the use of the PGD method for the analysis of plates can be recommended when performing detailed analysis of through-thickness variations, such as interlaminar stresses in composite laminates or the study of the out-of-plane variations in cracked plates, as in the present work. Moreover, the PGD can incorporate the parametric study of some material and geometric parameters in a single analysis, treating them as additional coordinates. This will result in additional cost reductions not considered in Fig. 1.

In this work, this approach is extended to cracked plates and, in addition, the separated representation is generalized for including material parameters and geometric dimensions, which are treated as extra-coordinates. The resulting problem becomes multidimensional but thanks to the separated representation the curse of dimensionality can be circumvented, and the general parametric solution is computed only once and in a very efficient way.

Since the 3D nature of the elastic fields in a plate problem with a straight-through crack is essentially dependent on the Poisson's ratio ν and the plate thickness B, the proposed PGD approximation to the solution is solved introducing ν and B as extra-coordinates. The components of the displacement field u_j are searched under the following separated approximation, in a fashion similar to that presented in Chinesta et al. (2011a):

$$u_j(x,y,z,\nu,B) \approx \sum_{i=1}^{n} u^i_{j,xy}(x,y) \cdot u^i_{j,z}(z) \cdot u^i_{j,\nu}(\nu) \cdot u^i_{j,B}(B) \tag{3}$$

where the second subscript refers to each of the separated functions. It is convenient to express this approximation in vector form as follows:

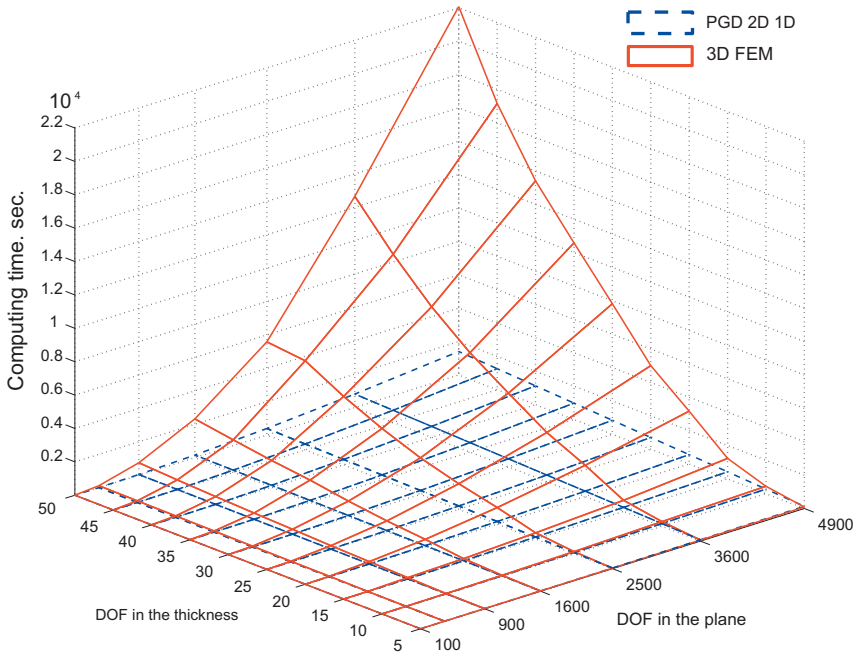

Fig. 1. Comparison of computational costs for different discretizations when solving a plate problem using the PGD approach and the standard 3D FEM.

$$\mathbf{u}(x,y,z,v,B) = \begin{Bmatrix} u_1(x,y,z,v,B) \\ u_2(x,y,z,v,B) \\ u_3(x,y,z,v,B) \end{Bmatrix} \approx \sum_{i=1}^{n} \mathbf{u}_{xy}^i(x,y) \circ \mathbf{u}_z^i(z) \circ \mathbf{u}_v^i(v) \circ \mathbf{u}_B^i(B) \tag{4}$$

where the symbol "$\circ$" is used to denote the so-called entry-wise, Hadamard or Schur multiplication for vectors (component-by-component multiplication). The approximated solution (4) enables the computation for different values of v and B in just a single analysis. In other problems of engineering, this capability has been successfully applied for on-line analysis, optimization or inverse analysis even on deployed platforms as proven in Bognet et al. (2012) and Ghnatios et al. (2012).

2.2. Formulation of the PGD as applied to cracked plates

In what follows, we present the essentials of the PGD formulation as applied to solve the cracked plate problem. For additional details concerning the separated representation constructor the interested reader can refer to Chinesta et al. (2010) and Chinesta et al. (2011b) and the references therein. We start from the weak form of a linear elastic problem in continuum solid mechanics:

$$\int_\Omega \boldsymbol{\varepsilon}(\delta\mathbf{u})^{\mathrm{T}} \mathbf{D} \boldsymbol{\varepsilon}(\mathbf{u})\, \mathrm{d}\Omega = \int_\Omega \delta\mathbf{u}^{\mathrm{T}} \mathbf{b}\, \mathrm{d}\Omega + \int_{\partial\Omega_{\mathrm{N}}} \delta\mathbf{u}^{\mathrm{T}} \mathbf{t}\, \mathrm{d}\partial\Omega \tag{5}$$

where Ω is the domain of the problem to be solved, subjected to Dirichlet boundary conditions on a region $\partial\Omega_{\mathrm{D}}$ and Neumann boundary conditions with surface tractions $\mathbf{t}$ on $\partial\Omega_{\mathrm{N}}$, such that $\partial\Omega_{\mathrm{D}} \cup \partial\Omega_{\mathrm{N}} = \partial\Omega$ and $\partial\Omega_{\mathrm{D}} \cap \partial\Omega_{\mathrm{N}} = \emptyset$. $\boldsymbol{\varepsilon}$ denotes the engineering strain vector, $\mathbf{D}$ is the elastic stiffness constitutive matrix, $\mathbf{b}$ represents the external body forces per unit volume and $\delta\mathbf{u}$ is any virtual variation of the displacement field $\mathbf{u}$ that is compatible with the prescribed boundary conditions on $\partial\Omega_{\mathrm{D}}$.

In the formulation of the PGD, we assume that the displacement field is approximated by (4). This approximated solution is generated by adding new terms (or modes). Let us assume that we already know the first n modes of the approximated solution and we are interested in adding a new term $n+1$:

$$\begin{aligned} \mathbf{u}(x,y,z,v,B) &\approx \sum_{i=1}^{n} \mathbf{u}_{xy}^i(x,y) \circ \mathbf{u}_z^i(z) \circ \mathbf{u}_v^i(v) \circ \mathbf{u}_B^i(B) + \mathbf{Q}_{xy}(x,y) \\ &\quad \circ \mathbf{R}_z(z) \circ \mathbf{S}_v(v) \circ \mathbf{T}_B(B) \\ &= \mathbf{u}_n + \mathbf{Q}_{xy}(x,y) \circ \mathbf{R}_z(z) \circ \mathbf{S}_v(v) \circ \mathbf{T}_B(B) \end{aligned} \tag{6}$$

where $\mathbf{Q}_{xy}, \mathbf{R}_z, \mathbf{S}_v, \mathbf{T}_B$ are unknown terms of the separated functions $\mathbf{u}_{xy}, \mathbf{u}_z, \mathbf{u}_v, \mathbf{u}_B$ for that mode, respectively. Since the first n modes are already determined at this stage, the admissible variation of the displacement field is:

$$\delta\mathbf{u}(x,y,z,v,B) = \delta(\mathbf{Q}(x,y) \circ \mathbf{R}(z) \circ \mathbf{S}(v) \circ \mathbf{T}(B)) \tag{7}$$

Substituting into the weak form (5) and omitting the symbol "$\circ$" in subsequent equations for the sake of compactness:

$$\begin{aligned} \int_\Omega \boldsymbol{\varepsilon}(\delta(\mathbf{QRST}))^{\mathrm{T}} \mathbf{D} \boldsymbol{\varepsilon}(\mathbf{QRST})\, \mathrm{d}\Omega &= -\int_\Omega \boldsymbol{\varepsilon}(\delta(\mathbf{QRST}))^{\mathrm{T}} \mathbf{D} \boldsymbol{\varepsilon}(\mathbf{u}_n) \\ &\quad + \int_\Omega (\delta(\mathbf{QRST}))^{\mathrm{T}} \mathbf{b}\, \mathrm{d}\Omega \\ &\quad + \int_{\partial\Omega_{\mathrm{N}}} (\delta(\mathbf{QRST}))^{\mathrm{T}} \mathbf{t}\, \mathrm{d}\partial\Omega \end{aligned} \tag{8}$$

where the first term on the right hand side of the equation corresponds to the contribution of the first n modes already available, being $\mathbf{u}_n$ the summation of these n modes given in (6).

On the other hand, the engineering strain vector involves the first derivatives of $\mathbf{u}$ and when applied to the new mode to be found yields:

$$\boldsymbol{\varepsilon}(\mathbf{Q}_{xy}\mathbf{R}_z\mathbf{S}_v\mathbf{T}_B) = \begin{Bmatrix} Q_{xy,x}^{u_1} R_z^{u_1} S_v^{u_1} T_B^{u_1} \\ Q_{xy,y}^{u_2} R_z^{u_2} S_v^{u_2} T_B^{u_2} \\ Q_{xy}^{u_3} R_{z,z}^{u_3} S_v^{u_3} T_B^{u_3} \\ Q_{xy,y}^{u_1} R_z^{u_1} S_v^{u_1} T_B^{u_1} + Q_{xy,x}^{u_2} R_z^{u_2} S_v^{u_2} T_B^{u_2} \\ Q_{xy}^{u_1} R_{z,z}^{u_1} S_v^{u_1} T_B^{u_1} + Q_{xy,x}^{u_3} R_z^{u_3} S_v^{u_3} T_B^{u_3} \\ Q_{xy}^{u_2} R_{z,z}^{u_2} S_v^{u_2} T_B^{u_2} + Q_{xy,y}^{u_3} R_z^{u_3} S_v^{u_3} T_B^{u_3} \end{Bmatrix} \tag{9}$$

The superscripts indicate the corresponding components of the displacement field and the second subscripts denote the customary derivatives with respect to the spatial coordinates. Upon substitution into (8) and after routine algebra, the terms can be grouped for each of the separated variables, arriving to an expression of the form:

$$\int_{xy} \delta Q^{u_1}_{xy,x} Q^{u_1}_{xy,x} \mathrm{d}x\mathrm{d}y \cdot \int_z \delta R^{u_1}_z R^{u_1}_z \mathrm{d}z \cdot \int_v \delta S^{u_1}_v D_{11}(v) S^{u_1}_v \mathrm{d}v \cdot \int_B \delta T^{u_1}_B T^{u_1}_B \mathrm{d}B + \cdots = -\int_\Omega \boldsymbol{\varepsilon}(\delta(\mathbf{QRST}))^{\mathrm{T}} \mathbf{D}\boldsymbol{\varepsilon}(\mathbf{u}_n) + \int_\Omega (\delta(\mathbf{QRST}))^{\mathrm{T}} \mathbf{b}\,\mathrm{d}\Omega + \int_{\partial\Omega_{\mathrm{N}}} (\delta(\mathbf{QRST}))^{\mathrm{T}} \mathbf{t}\,\mathrm{d}\partial\Omega \tag{10}$$

Note that the elements of the stiffness matrix, D_{ij}, depend on the Poisson's ratio and, therefore, D_{11} has been grouped in the corresponding integral in (10).

The solution for the sought functions $\mathbf{Q}_{xy}, \mathbf{R}_z, \mathbf{S}_v$ and $\mathbf{T}_B$ is searched by iteration using the fixed point method, due to both its easy of implementation and good convergence properties. Assume that an initial guess is given for the functions $\mathbf{R}_z, \mathbf{S}_v$ and $\mathbf{T}_B$ and their contribution for each summand on the left hand side of (10) is termed α_1, α_2, etc. Then, an estimation for $\mathbf{Q}_{xy}$ can be obtained by solving a standard weak form on $\mathbf{Q}_{xy}$:

$$\alpha_1 \int_{xy} \delta Q^{u_1}_{xy,x} Q^{u_1}_{xy,x} \mathrm{d}x\mathrm{d}y + \cdots = -\int_\Omega \boldsymbol{\varepsilon}(\delta(\mathbf{Q})\mathbf{RST})^{\mathrm{T}} \mathbf{D}\boldsymbol{\varepsilon}(\mathbf{u}_n) + \int_\Omega (\delta(\mathbf{Q})\mathbf{RST})^{\mathrm{T}} \mathbf{b}\,\mathrm{d}\Omega + \int_{\partial\Omega_{\mathrm{N}}} (\delta(\mathbf{Q})\mathbf{RST})^{\mathrm{T}} \mathbf{t}\,\mathrm{d}\partial\Omega \tag{11}$$

In this work, this weak form is solved numerically in the 2D domain (x, y) by using a 2D finite element approximation, after introducing the corresponding discretization. Once the estimation for $\mathbf{Q}_{xy}$ is available, the functions $\mathbf{R}_z, \mathbf{S}_v$ and $\mathbf{T}_B$ are, in turn, estimated analogously. Note that these functions are solved in their corresponding 1D spaces using 1D finite element discretizations and, therefore, their numerical approximation is computationally inexpensive. The process is repeated iteratively until convergence of the $n+1$ mode of the displacement approximation (6), i.e. until $||\mathbf{u}_{n+1} - \mathbf{u}_n|| < \epsilon$, where ϵ is a prescribed tolerance.

The convergence of the method was proved for symmetric and positive definite differential operators in Bris et al. (2009) and Ammar et al. (2010). In the general case, as the one addressed here in which new coordinates have been introduced, the convergence has been always attained in the numerous tests carried out until now, including other problems in engineering. However, at present there is not a mathematical proof of such convergence. To date, convergence of the PGD has been observed for all the general elliptic or parabolic problems tested, and the technique has also been successfully applied in the case of hyperbolic equations (Huerta, 2011; Barbarulo, 2012). Thus, from our numerical experiments reported in Chinesta et al. (2011b), the efficiency and robustness of the solvers based on the construction of separated representations have been verified.

The nonlinear problem involved in each enrichment step can be addressed by using any appropriate linearization strategy. In Ammar et al. (2006) and Ammar et al. (2007) the Newton's strategy was considered. The simple alternated direction fixed point algorithm used in this work is efficient and robust despite its simplicity. Moreover, we have observed that the converged solution does not depend on the initial guess and the convergence rate does not depend significantly on that choice. In this work, all the initial guesses are random vectors. Based in our experience, the best convergence (with respect to the number of fixed point iterations at a given enrichment step) is actually observed for random initial guesses which excite all the modes of the operator.

2.3. Computation of the J-integral

The great advantage of obtaining a displacement approximation of the form $\mathbf{u}(x, y, z, v, B)$ is that a 3D problem plus two additional coordinates is solved in a single analysis. Postprocessing for given values of the spatial coordinates and of the parameters v and B within the range of their domains of definition is immediate. Therefore, the displacement field at the nodal grid 2D $\times$ 1D is available as in a standard FE solution and the strain and stress fields can also be derived.

Our objective in the work is to demonstrate the effectiveness of the PGD to solve a 3D crack in an elastic plate. In general, two types of singularity coexist in a cracked 3D plate with free boundaries: the classical Williams solution ($r^{-0.5}$ singularity) and the corner or vertex singularity. Therefore, we have provided comparisons to both the Williams solution and the corner singularity computed by Benthem as a function of the Poisson's ratio (the latter, for the straight-through crack problem only). The comparison of the Williams solution has been performed in terms of the pointwise J-integral, which is directly related to the stress intensity factors, and therefore it characterizes the Williams contribution to the solution. The use of the pointwise J-integral for a 3D crack problem is widely acknowledged in the literature (e.g. Li et al. (1985), Newman and Raju (1983) and Nakamura and Parks (1988)).

In this work, we use the J-integral as a scalar functional to measure the quality of the Williams solution. The J-integral is a quantity of interest in fracture mechanics that it is defined pointwise at each position of the crack front in 3D problems, $J = J(s)$, where s is a parametric coordinate along the crack front, see Fig. 2. The computation of $J(s)$ has been performed using an equivalent domain integral, as proposed by Li et al. (1985) and Shih et al. (1986) (deLorenzi (1982, 1985), obtained exactly the same result using the concept of virtual crack extension and a consistent continuum mechanics approach):

$$J(s) \approx J_{\mathrm{vol}} = \frac{\Delta a}{A_c} \int_V \left(\sigma_{ij} \frac{\partial u_j}{\partial x_1} - W\delta_{1i} \right) \frac{\partial q_1}{\partial x_i} \mathrm{d}V \tag{12}$$

where W is the strain energy density, δ_{ij} is the Kronecker's delta, Δa is a virtual crack extension at a point s of the crack front (see Fig. 2), A_c is the virtual increment in crack area generated by the virtual crack extension, and q_1 is a continuous weight function that varies between 0 and 1 and scales the virtual crack extension Δa within the crack front segment Δs. The fields are expressed in the local coordinate system of axes x_1, x_2, x_3 shown in Fig. 2. The volume of integration V must surround the crack front from one crack face to the other and its width at the crack front is Δs. Note that the value of the volume integral J_{vol} is indeed an approximation to the pointwise value $J(s)$, since Δs is finite. In the context of the standard FEM, it is well known that the computation of J as a domain (volume) integral is numerically advantageous, as it becomes unnecessary to capture the details of the singular field near the crack front. In addition, it tends to provide more accurate results than the equivalent contour integral, because it involves information evaluated in a domain instead of a contour. An important advantage of the method is that, theoretically, the value of $J(s)$ is independent of the domain chosen, although discretization errors present in the vicinity of the crack front force to avoid small domains surrounding the crack front.

The same advantages and recommendations apply when computing $J(s)$ from a PGD solution. We have performed the integration over V by defining volume cells that would match the 3D finite elements that could be constructed by the underlying 2D $\times$

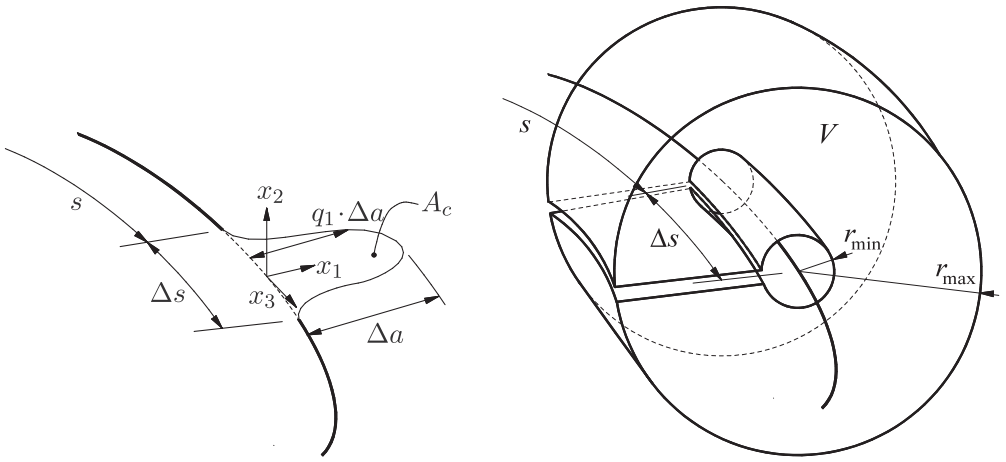

Fig. 2. Virtual crack extension of a crack front segment Δs for the application of the EDI method.

1D nodal grid. In this work, we will only deal with mode I examples and hence the pointwise value of the mode I stress intensity factor K_I (SIF) can be calculated using the following expression:

$$K_I(s) = \sqrt{J(s)\frac{E}{1-\nu^2}} \tag{13}$$

where E is the Young's modulus and ν the Poisson's ratio.

3. Numerical verification

In this section, two problems are analyzed to verify the performance of the PGD to solve cracked plates. The first problem involves a straight-through crack front, with a discretization that enables to capture the corner singularity with high accuracy at a low computational cost and, at the same time, providing solutions for a range of ν and B. The convergence of the method with an increasing number of modes is also evidenced by comparison to a standard finite element solution. A quarter-elliptical corner crack in a plate is also solved, showing that the application of the PGD is not limited to straight-through crack fronts. In this latter case, the validation is restricted to the Williams part of the solution, since reference solutions for the corner singularity are not available for this geometry.

3.1. Plate with a straight-through crack

3.1.1. Problem description

Fig. 3 is a sketch of the geometrical model of a plate with a straight-through crack. It represents a plate of thickness B with a single edge crack of length $a/W = 0.5$. The plate is loaded with uniform tension σ. The particular dimensions of the model are $W = 2,\ H = 6$ [units of length]. As the thickness B is an independent parameter included in the PGD formulation, it is solved for the range $B/2 \in [0.5, 10]$. Symmetry conditions are applied on the ligament (plane xz) and on the midplane (parallel to the plane xy). The material model is linear elastic, with $E = 207{,}000$ [units of pressure], being ν solved in the range $\nu \in [0, 0.49]$ as an independent parameter. Note that the origin of the global system of reference is located at the intersection of the crack front and the free surface, where the corner singularity exists.

The discretizations for the space domain in the xy plane (2D domain) and in the z direction (1D domain) are shown in Fig. 4. The elements are conveniently refined towards the crack tip and towards the crack front corner, respectively. The 2D discretization is composed of 7031 linear triangular elements. The mesh was

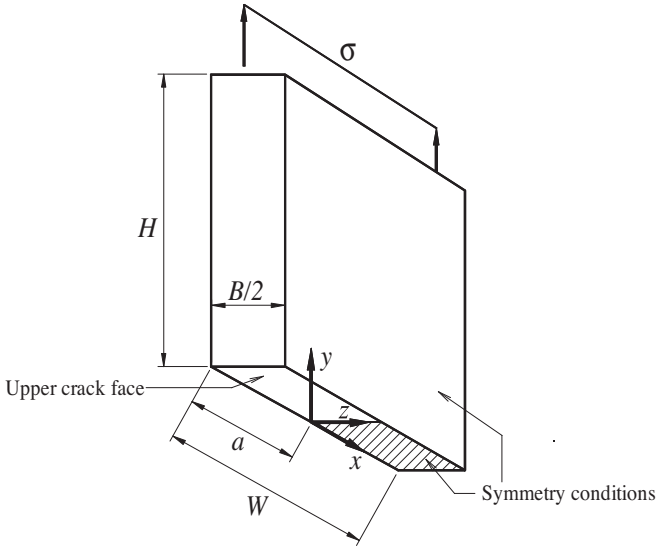

Fig. 3. Model of a plate with a single edge crack loaded in tension.

h-adapted by refining a previous 2D analysis to optimize the 2D discretization (it is plotted in the deformed shape to show the crack location). The 1D mesh is composed of 42 2-node linear elements. Note that the equivalent 3D discretization using prisms of triangular base amounts to 295,302 elements, which is a large number when compared to the number of elements in the 2D or 1D discretization. The discretization of the ν and B spaces is performed using 1D FE discretizations with two-node elements in increments of 0.01 in the range $\nu \in [0, 0.49]$ and in increments of 0.1 in the range $B/2 \in [0.5, 10]$ for the B-space. This would correspond to a very large number of 3D solutions if they were to be solved with a standard FE approach, since it would be necessary to perform 4800 3D standard FE analyses to obtain the solutions in the range $\nu \in [0, 0.49]$ times the range of variation of $B/2 \in [0.5, 10]$ given their respective increments.

3.1.2. J-integral along the crack front

In this problem, we have computed $J(z)$ through (12), using an annular q-function at each location, defined by a ring with $r_{min} = 0.5 \cdot 10^{-3}$ and $r_{max} = 4 \cdot 10^{-3}$ units, as indicated in Fig. 2. The q-function decays linearly in the z direction at both sides of the extraction location within the calculation ring (except at the free surface and midplane locations, where q decays linearly at

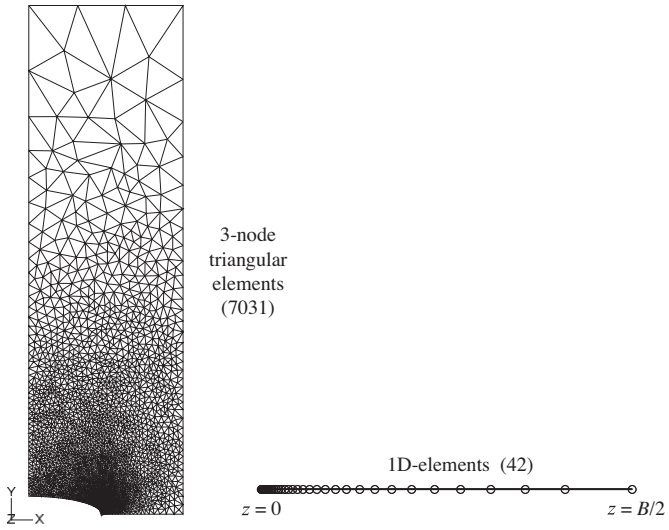

Fig. 4. 2D and 1D discretizations of the space domain $(x,y) \times z$.

one side only). Fig. 5 shows the results obtained for the J-integral along the crack front, particularized for the case $B/2 = 1$ and $\nu = 0.3$. Note that the bottom plot is an enlarged view of the zone near the corner singularity. It can be observed that $J(z)$ exhibits the expected behavior reported in the literature (e.g. Nakamura and Parks, 1988) with a maximum at the midplane and decaying to zero at the corner point. The PGD solution has been obtained calculating $n = 30$ modes for the approximation (4). Note that the PGD provides virtually the same results as a standard FEM analysis with the same discretization (295302 linear prisms, about $4.7 \cdot 10^5$ dofs), even in the vicinity of the corner point, at a much lower computational cost and including in the single solution the results for any choice of B and ν in their respective intervals of variation. In Fig. 5 another FE solution is included as reference solution, computed with a very refined mesh with more than $2.3 \cdot 10^6$ degrees of freedom using 20-node hexahedrons and 160 elements along the crack front, which differs from the PGD solution and the other FE solution mainly due to the discretization error.

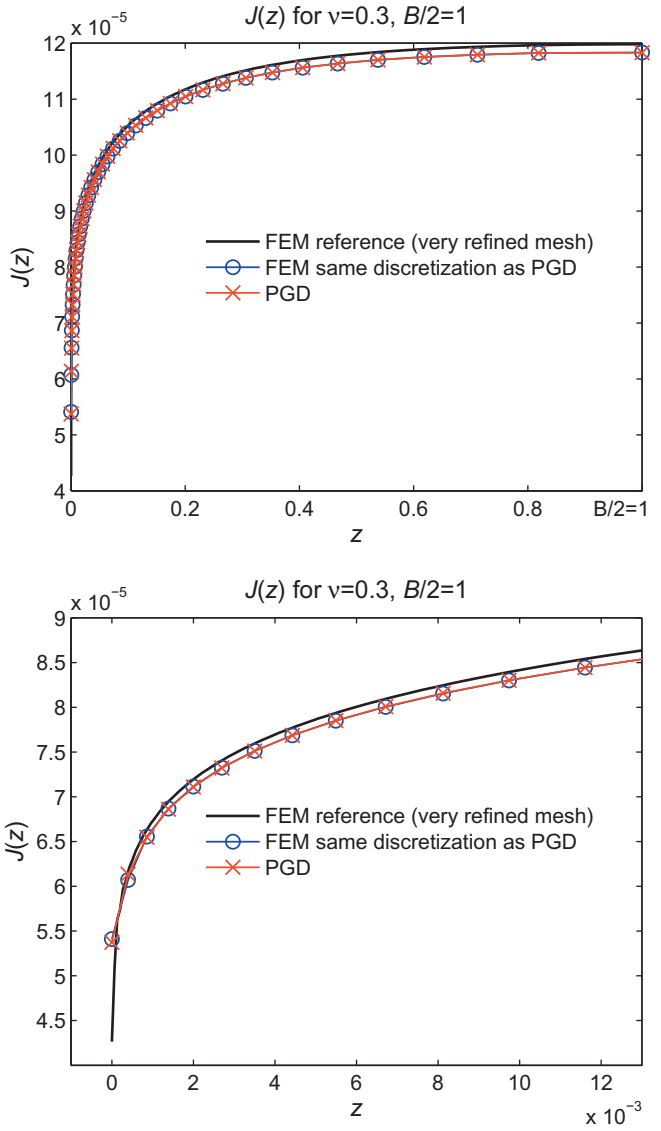

Fig. 5. Pointwise value of the J-integral along the crack front for the case $B/2 = 1$ and $\nu = 0.3$. Bottom: enlarged view near the corner point.

3.1.3. Convergence with number of modes n

Fig. 6 exemplifies the convergence of the PGD solution with the number of modes n. As the number of modes in the approximation (4) increases, the PGD solution converges towards the equivalent FE solution obtained with the same discretization. In other words, the FE solution is the best possible solution for a given discretization. In our example, sufficient accuracy is attained with $n = 30$ modes.

Having fixed $B/2 = 1$ and $\nu = 0.3$, the solution with a single mode $n = 1$ corresponds to the approximation $\mathbf{u}(x,y,z) \approx \mathbf{u}_{xy}(x,y) \circ \mathbf{u}_z(z)$, which means that the solution of the 2D space domain is fully decoupled from the z direction. It is very interesting to note that the PGD solution for $n = 1$ matches the 2D plane strain solution computed for the 2D domain. In this problem, the 2D plane strain solution is the only physical solution for which the 2D solution is independent of the z direction and, as a result, the PGD converges to it when only a single mode is allowed. Fig. 6 also shows that the successive addition of modes modify the plane strain solution to account for the corner singularity effect.

3.1.4. J-integral for different values of the Poisson's ratio

In this section, we benefit from the single PGD solution for different values of the material parameter ν. The solution has been found for the range $\nu \in [0, 0.49]$ using a 1D FE mesh at increments of 0.01 and can be interpolated to any other value within this interval. Fig. 7 shows five representative solutions. The case $\nu = 0$ implies that all normal strains are uncoupled (there is no Poisson's effect). As a consequence, no corner singularity effect arises and the $J(z)$ solution is constant along the thickness. For an in-plane loading such the one applied in this example, there is no strain in the z direction and the case $\nu = 0$ can be considered a plane strain problem. At the same time, no stress triaxiality is induced in the crack front vicinity and the solution for $\nu = 0$ can also be considered a plane stress solution. As a consequence, the case $\nu = 0$ is the only one for which a truly plane stress solution can exist in the whole 3D domain, being simultaneously a plane strain solution.

For any $\nu > 0$, the different contractions in the z direction, i.e. differences in the out-of-plane strain ε_z, in the most loaded region near the crack front (ligament) and the less loaded region (crack face), induce a state of stress triaxialiaty ($\sigma_z \neq 0$) in the interior region of the plate that must vanish at the free plate surface. As a consequence, a corner or vertex singularity arises. Fig. 7 shows that, the larger the value of ν, the larger the extent of this effect. Note that for a typical value $\nu = 0.3$, this effect modifies

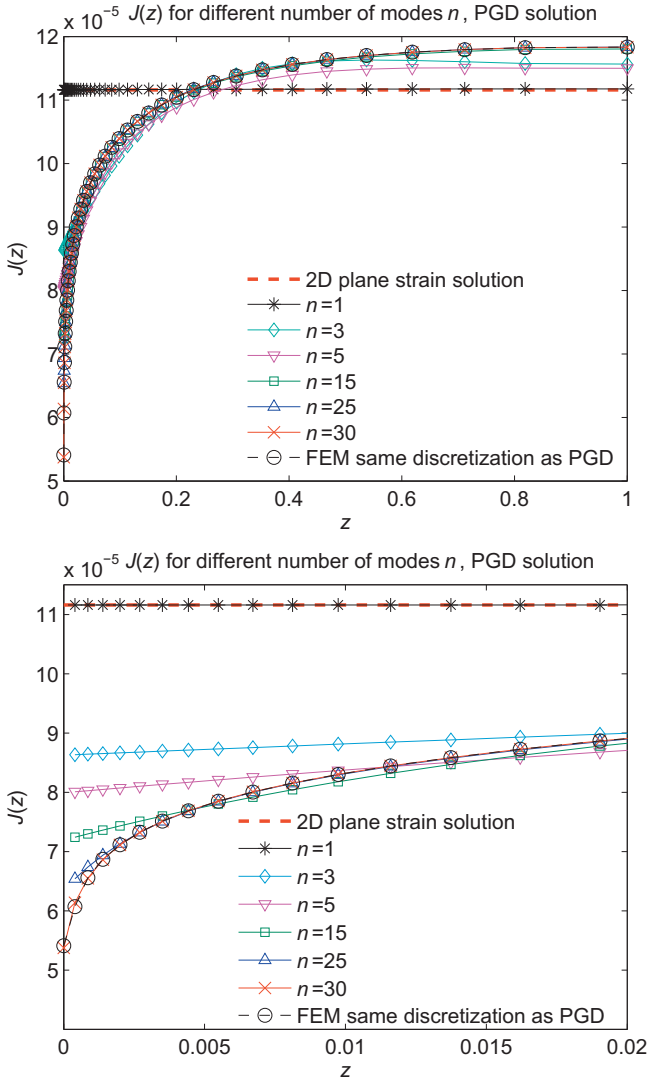

Fig. 6. Convergence of the PGD solution with an increasing number of modes. Case $B/2 = 1$ and $\nu = 0.3$. Bottom: enlarged view near the corner point.

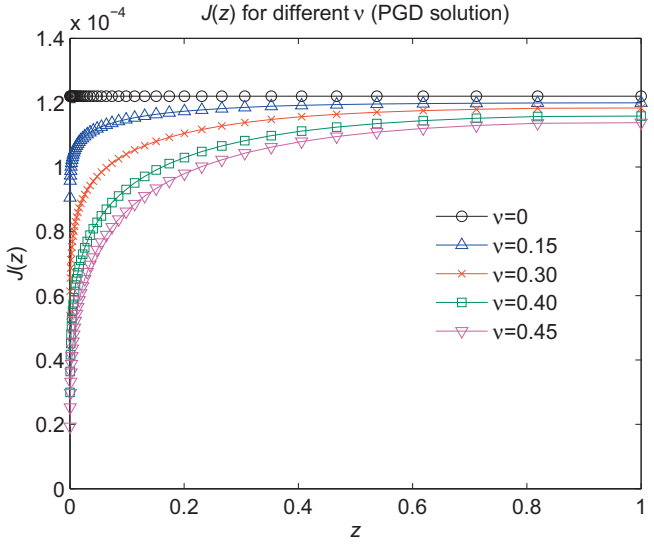

Fig. 7. $J(z)$ for different values of the Poisson's ratio ν. PGD solution. Case $B/2 = 1$.

the distribution of J in a region of about 40% of the half-thickness measured from the free plate surface ($z = 0$).

Thanks to the refined discretization in the z direction, computationally affordable by the PGD, the zone dominated by the corner singularity has been conveniently captured. Fig. 8 shows a log–log plot of the value of the stress intensity factor along the crack front computed through (13). The straight portions of the plots indicate the extent of the corner singularity dominated zone (about 10% of the half thickness), in agreement with Benthem's prediction, who showed that (Benthem, 1977):

$$K(z) \propto z^{\lambda_B(\nu)+0.5} \quad \text{when} \quad z \to 0 \tag{14}$$

where λ_B is the exponent computed by Benthem that depends on ν. Table 1 compares the slopes obtained in this work from the PGD solutions and the values predicted by Benthem, showing a very good agreement. This analysis also verifies Benthem's results, obtained under a half-infinite domain hypothesis. We note in passing that, although these results are accepted in the literature, they have been questioned in some numerical works due to the lack of enough FE discretization.

3.1.5. J-integral for different thicknesses

The formulation for the PGD considered in this work also includes the thickness B as a parameter in the solution. This parameter takes values within the interval $B/2 \in [0.5, 10]$ that is discretized using a 1D FE element mesh and the corresponding interpolation, thus benefiting from the versatility of the PGD approach with a single analysis. Fig. 9 shows the variation of the pointwise $J(z)$ along the crack front for four different thicknesses and $\nu = 0.3$ (results are plotted versus normalized thickness). It can be observed that the thickness also influences the shape of the $J(z)$ distribution, being B/a the relevant parameter. The distribution changes from a single maximum at the midplane for small B/a ratios to a couple of maxima in the vicinity of the free boundaries for the whole thickness and large B/a ratios. This behavior is in good agreement with the study presented in Giner et al. (2010).

3.2. Plate with a straight-through crack solved with 1D-discretization in the y-direction

To verify the performance of the PGD with other types of discretizations, the same problem has been solved with a 2D discretization in the xz plane combined with a 1D discretization in

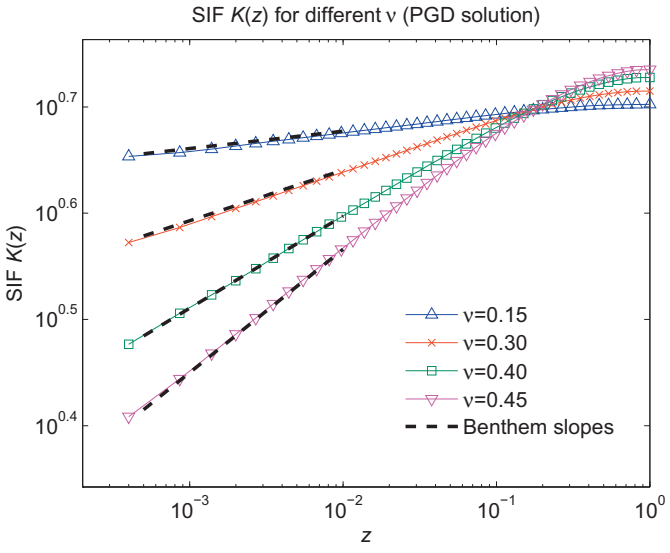

Fig. 8. Log–log plot for computing slopes from the stress intensity factor solutions along the crack front, $K(z)$. PGD results for different values of ν. Case $B/2 = 1$.

Table 1
Values of the slopes from the PGD solutions shown in Fig. 8 compared to the values derived from Benthem's exponents. Case $B/2 = 1$.

ν	Log–log slope	$\lambda_B + 0.5$
0.15	0.017	0.016
0.30	0.049	0.048
0.40	0.087	0.087
0.45	0.116	0.116

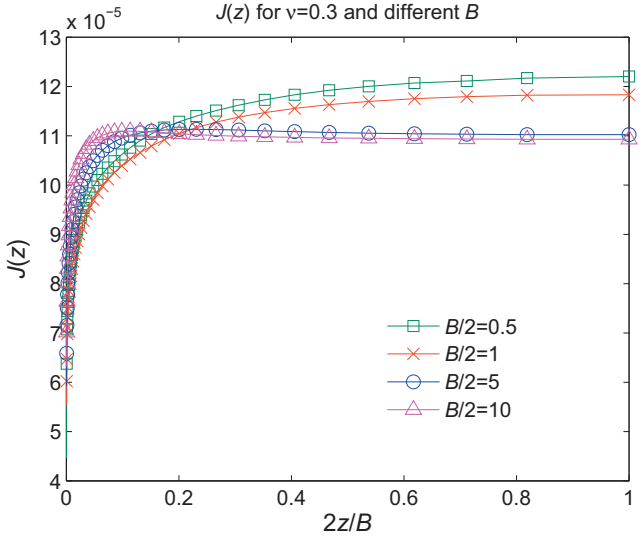

Fig. 9. Pointwise value of the J-integral along the crack front for $\nu = 0.3$ and different values of B vs. normalized thickness.

the y-direction, as shown in Fig. 10. In this case bilinear quadrilateral elements for the 2D mesh have been used.

When applying the PGD technique, this option has the additional difficulty that a portion of the xz plane must be constrained in the y-direction (ligament) whereas the crack face must remain free. This has been accomplished by using a penalty approach to impose the boundary constraint on the ligament region. Fig. 11 shows the results obtained with this new discretization compared to the previous results presented in Fig. 5. It can be observed that the discretization using bilinear quadrilaterals in the xz plane tends to provide good results, virtually matching the reference solution obtained with a very refined mesh with 20-node hexahedra.

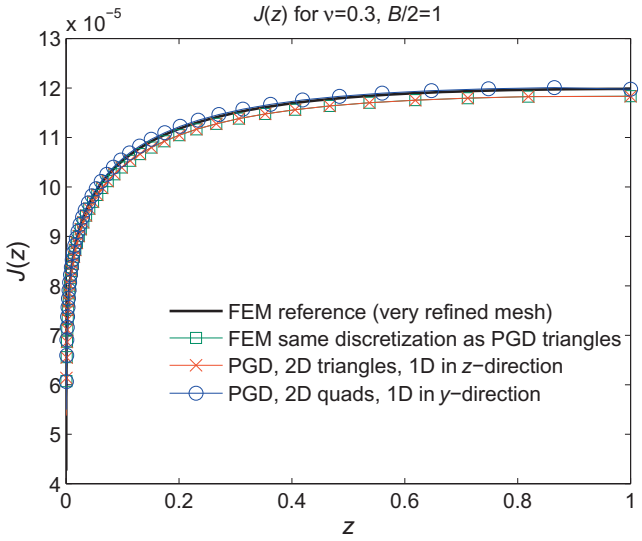

Fig. 11. Pointwise value of the J-integral along the crack front for $B/2 = 1$ and $\nu = 0.3$. Same results as in Fig. 5 including 2D discretization with quadrilaterals and 1D discretization in y-direction.

3.3. Plate with a quarter-elliptical corner crack

The possibility of discretizing the crack plane with the 2D discretization, as verified in the previous section, paves the way for the solution of planar cracks with curved crack fronts. In this section, a quarter-elliptical corner crack (see Fig. 12) is modelled using 4-node quadrilaterals in the xz plane plus a 1D discretization in the y-direction, as shown in Fig. 13. The particular dimensions of the model are $t = 1$, $a = 0.5$, $c = 1.25$, $h = w = 6.25$, which correspond to the ratios $a/c = 0.4$, $a/t = 0.5$. The material properties are the same as in the previous example, with $\nu = 0.3$. A solution to this case was provided by Newman and Raju (1983) using the standard FEM, which will be taken here as a reference solution. Newman and Raju's numerical solution (N&R) is given with an accuracy of 5% and is valid for $\nu = 0.3$ and for a ratio $c/w \leqslant 0.2$ (c/w is exactly 0.2 in our case). The solution to this problem can also be found in e.g. Murakami and ed. (1987). Newman and Raju (1983) reported some point values using FE analyses and a fitted equation for a wide range of ϕ, i.e. the position angle defined in Fig. 12. These solutions are reproduced in Fig. 14.

Fig. 14 also shows the PGD results for the stress intensity factor K_I along the crack front. The PGD results exhibit the same trend as

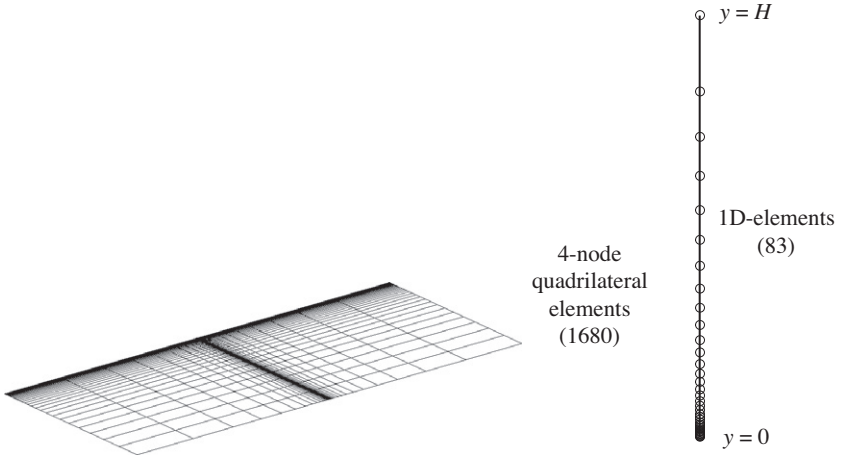

Fig. 10. 2D and 1D discretizations of the space domain $(x,z) \times y$ for the same problem of Fig. 3.

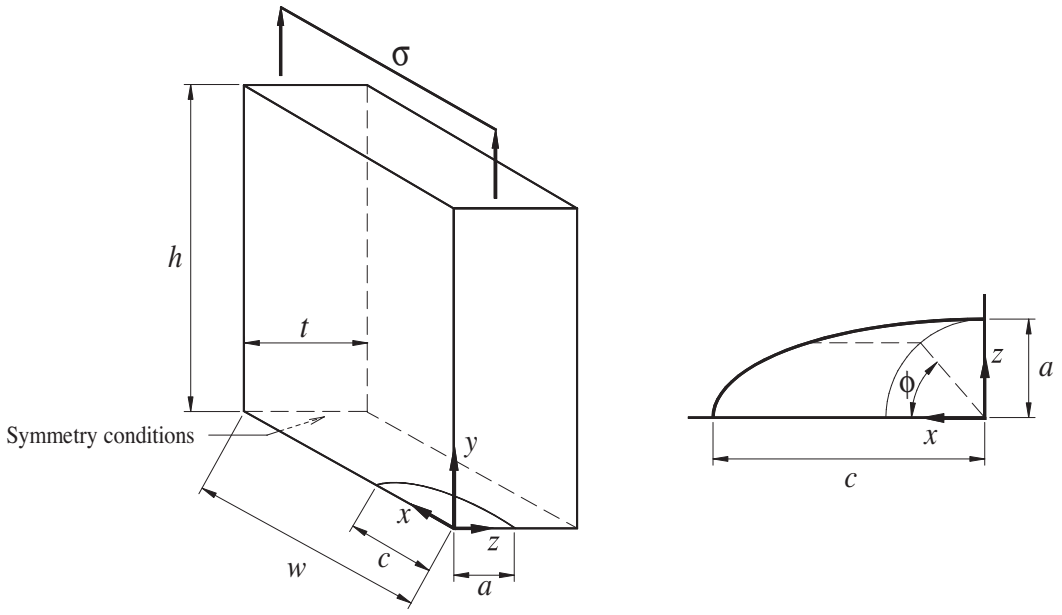

Fig. 12. Geometrical model of a quarter-elliptical corner crack. Convention for measuring the position angle ϕ.

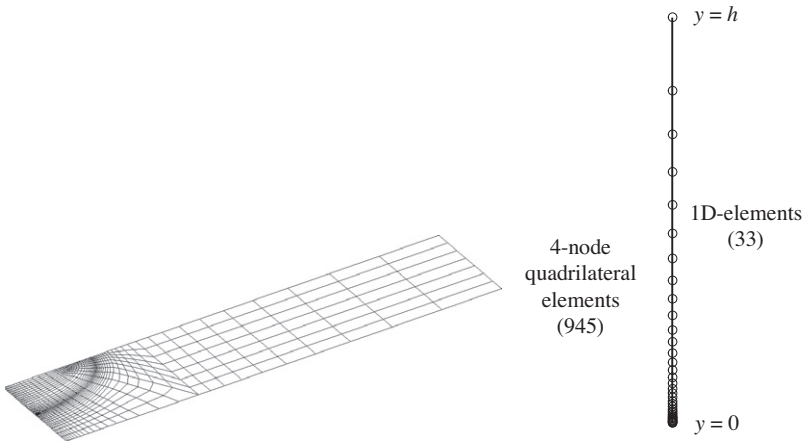

Fig. 13. Quarter-elliptical corner crack. 2D and 1D discretizations of the space domain $(x,z) \times y$.

the N&R's solution, although the PGD values are slightly greater, lying within the 5% relative error. Other recent works that solve analogous problems with the FE method (e.g. González-Albuixech et al. (2011)) also yield values above those of the N&R's solutions.

Note that the PGD solution also tends to capture the free boundary effect, evidenced by a decaying value of K_I, especially in the neighborhood of $\phi = \pi/2$. The effect at this corner is more manifest because, in this region, the crack front closely approximates a straight crack front intersecting a free boundary. This effect was also reported in Newman and Raju (1983) for a similar geometry using several refined meshes.

3.4. Convergence of the numerical solutions

The number of PGD modes to achieve an accurate solution depends largely on the type of problem and, therefore, the number of modes cannot be estimated *a priori* to ensure that the computed solution is accurate enough. As commented at the end of Section 2.2, the convergence check consists in computing the relative residual of the problem considered. Then, the iterative enrichment process keeps running until the relative residual of the problem is smaller than a prescribed tolerance.

Fig. 15 shows the exact error between the full 3D FEM solution and the PGD solution on the same equivalent mesh as a function of the prescribed tolerance of the PGD problem. This error is computed as the integral over the whole domain of the relative error between the PGD solution and the 3D FEM solution using the energy norm. As can be noticed, the reduction of the prescribed tolerance is a good indicator of the accuracy of the solution because the integral of the relative error decreases very rapidly when the prescribed tolerance is reduced, i.e. the convergence is quite fast.

Fig. 16 shows the number of modes in the PGD solution for the numerical examples. As expected, the number of modes needed to describe the solution increases with the required accuracy. Moreover, the parameterized solution including the thickness B and the Poisson's ratio ν as coordinates needs many more modes to capture the complexity of the solution. However, the accuracy is quite similar in comparison with non-parametric solutions. In practice, a prescribed tolerance of 10^{-3} can be used for conventional engineering applications, which implies that less than 50

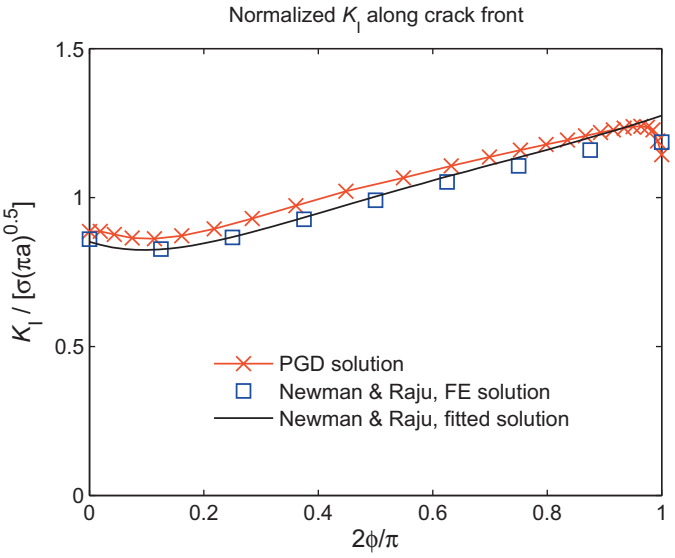

Fig. 14. Normalized stress intensity factor solutions along the crack front. PGD results compared to results given by Newman and Raju (1983).

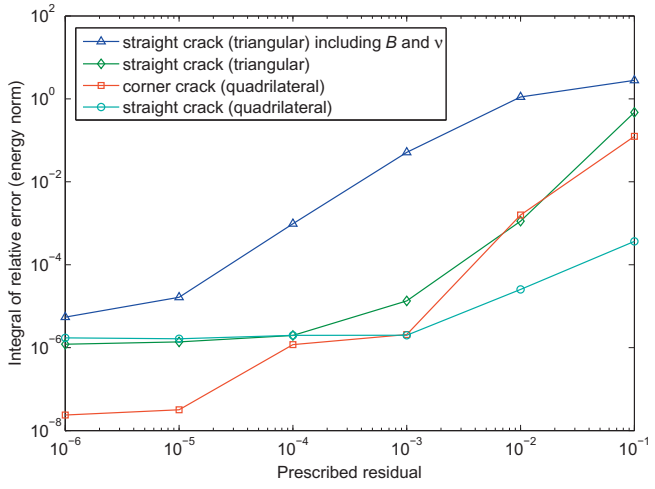

Fig. 15. Exact error between the full 3D FEM solution and the PGD solution on the same equivalent mesh as a function of the prescribed tolerance.

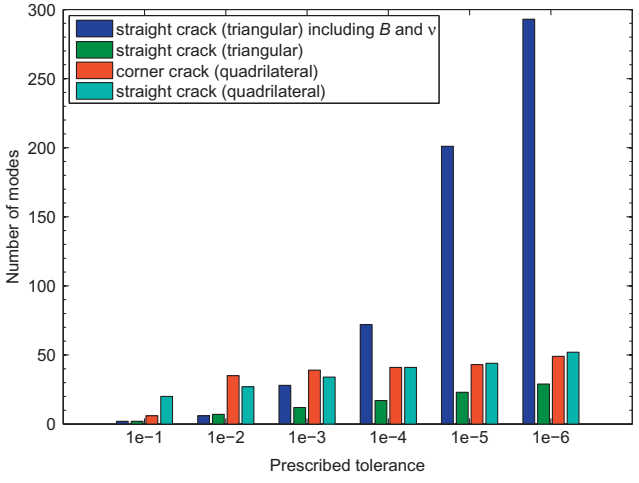

Fig. 16. Number of modes in the PGD solution for the numerical examples.

modes are included in the approximated solutions of the presented examples.

4. Conclusions

In this work, a formulation of the Proper Generalized Decomposition (PGD) for solving efficiently 3D cracked plates has been presented. For plate geometries, the space domain can be separated into a 2D discretization plus a 1D discretization. Moreover, certain material and geometry parameters that can be of interest for fracture mechanics problems have been included in the approximating space of the solution, namely the Poisson's ratio and the plate thickness. These parameters are considered as independent coordinates that take values within their respective intervals of definition. Thus, a single solution for a 3D elastic problem plus two additional coordinates can be obtained simultaneously in the space (x, y, z, ν, B). The method provides large computational cost reductions when compared to standard FE 3D analysis, not to mention the parametric variation of ν and B, and it also captures conveniently the crack front and corner singularities.

By means of numerical examples, it has been shown that very accurate results can be obtained with a reduced computational cost, including the variation with the parameters ν and B. The accuracy of the results has been measured in terms of the J-integral and the stress intensity factor K that are the main quantities of interest in linear elastic fracture mechanics. The intensity of the corner singularity has also been estimated, correlating well with predictions available in the literature. It has also been shown that the procedure can be successfully applied to solve planar cracks with curved crack fronts with the above commented advantages.

Acknowledgements

The authors thank the Ministerio de Ciencia y Tecnología for the support received in the framework of the projects DPI2010-20990, DPI2010-20542 and to the Generalitat Valenciana, Programme PROMETEO 2012/023.

References

Ammar, A., Mokdad, B., Chinesta, F., Keunings, R., 2006. A new family of solvers for some classes of multidimensional partial differential equations encountered in kinetic theory modeling of complex fluids. Journal of Non-Newtonian Fluid Mechanics 139, 153–176.

Ammar, A., Mokdad, B., Chinesta, F., Keunings, R., 2007. A new family of solvers for some classes of multidimensional partial differential equations encountered in kinetic theory modeling of complex fluids. Part II: Transient simulation using space–time separated representations. Journal of Non-Newtonian Fluid Mechanics 144, 98–121.

Ammar, A., Chinesta, F., Falcó, A., 2010. On the convergence of a greedy rank-one update algorithm for a class of linear systems. Archives of Computational Methods in Engineering 17 (4), 473–486.

Anderson, T.L., 2005. Fracture Mechanics. Fundamentals and Applications, third ed. Taylor and Francis, Boca Raton, Florida.

Barbarulo, A., 2012. On a PGD model order reduction technique for mid-frequency acoustic, Ph.D Thesis, ENS Cachan, France.

Bažant, Z.P., Estenssoro, L.F., 1979. Surface singularity and crack propagation. International Journal of Solids and Structures 15, 405–426.

Benthem, J.P., 1977. State of stress at the vertex of a quarter-infinite crack in a half-space. International Journal of Solids and Structures 13, 479–492.

Bognet, B., Bordeu, F., Chinesta, F., Leygue, A., Poitou, A., 2012. Advanced simulation of models defined in plate geometries: 3D solutions with 2D computational complexity. Computer Methods in Applied Mechanics and Engineering 201–204, 1–12.

Broek, D., 1986. Elementary Engineering Fracture Mechanics, fourth ed. Martinus Nijhoff, Dordrecht, The Netherlands.

Chinesta, F., Ammar, A., Cueto, E., 2010. Recent advances and new challenges in the use of the Proper Generalized Decomposition for solving multidimensional models. Archives of Computational Methods in Engineering 17 (4), 327–350.

Chinesta, F., Ammar, A., Leygue, A., Keunings, R., 2011a. An overview of the Proper Generalized Decomposition with applications in computational rheology. Journal of Non-Newtonian Fluid Mechanics 166, 578–592.

Chinesta, F., Ladevèze, P., Cueto, E., 2011b. A short review on model order reduction based on Proper Generalized Decomposition. Archives of Computational Methods in Engineering 18, 395–404.
deLorenzi, H.G., 1982. On the energy release rate and the J-integral for 3-D crack configurations. International Journal of Fracture 19, 183–193.
deLorenzi, H.G., 1985. Energy release rate calculations by the finite element method. Engineering Fracture Mechanics 21 (1), 129–143.
Dimitrov, A., Andrä, H., Schnack, E., 2001. Efficient computation of order and mode of corner singularities in 3D-elasticity. International Journal for Numerical Methods in Engineering 52, 805–827.
Ghnatios, Ch., Masson, F., Huerta, A., Cueto, E., Leygue, A., Chinesta, F., 2012. Proper Generalized Decomposition based dynamic data-driven control of thermal processes. Computer Methods in Applied Mechanics and Engineering 213–216, 29–41.
Giner, E., Fernández-Zúñiga, D., Fernández-Sáez, J., Fernández-Canteli, A., 2010. On the J_{x_1}-integral and the out-of-plane constraint in a 3D elastic cracked plate loaded in tension. International Journal of Solids and Structures 47 (7–8), 934–946.
González-Albuixech, V.F., Giner, E., Fernández-Sáez, J., Fernández-Canteli, A., 2011. Influence of the t_{33}-stress on the 3-D stress state around corner cracks in an elastic plate. Engineering Fracture Mechanics 78 (2), 412–427.
Hartranft, R.J., Sih, G.C., 1969. The use of eigenfunction expansions in the general solution of three-dimensional crack problems. Journal of Mathematics and Mechanics 19 (2), 123–138.
Hartranft, R.J., Sih, G.C., 1970. An approximate three-dimensional theory of plates with application to crack problems. International Journal of Engineering Science 8, 711–729.
Heyder, M., Kolk, K., Kuhn, G., 2005. Numerical and experimental investigations of the influence of corner singularities on 3D fatigue crack propagation. Engineering Fracture Mechanics 72, 2095–2105.
Huerta, A., 2011. Efficiency and accuracy of PGD applied to a practical engineering wave propagation problem. First International Workshop on Reduced Basis, POD and PGD Model Reduction Techniques, Paris, France.
Kwon, S.W., Sun, C.T., 2000. Characteristics of three-dimensional stress fields in plates with a through-the-thickness crack. International Journal of Fracture 104, 291–315.
Ladevèze, P., 1999. Nonlinear Computational Structural Mechanics. Springer, New York.
Ladevèze, P., Neron, D., Passieux, J.-C., 2009. On multiscale computational mechanics with time–space homogenization. In: Multiscale Methods Bridging the Scales in Science and Engineering. In: Fish, J. (Ed.), . Space Time Scale Bridging Methods. Oxford University Press, pp. 247–282.
Ladevèze, P., Passieux, J.-C., Neron, D., 2010. The LATIN multiscale computational method and the proper generalized decomposition. Computer Methods in Applied Mechanics and Engineering 199 (21–22), 1287–1296.
Le Bris, C., Lelivre, T., Maday, Y., 2009. Results and questions on a nonlinear approximation approach for solving high-dimensional partial differential equations. Constructive Approximation 30, 621–651.
Leung, A.Y.T., Su, R.K.L., 1995. A numerical study of singular stress field of 3D cracks. Finite Elements in Analysis and Design 18, 389–401.
Leung, A.Y.T., Su, R.K.L., 1996. Order of the singular stress fields of through-thickness cracks. International Journal of Fracture 75, 85–93.
Li, F.Z., Shih, C.F., Needleman, A., 1985. A comparison of methods for calculating energy release rates. Engineering Fracture Mechanics 21 (2), 405–421.
Murakami, Y. (Ed.), 1987. Stress Intensity Factors Handbook, vol. 2. Pergamon Press, Oxford, pp. 712–722.
Nakamura, T., Parks, D.M., 1988. Three-dimensional stress field near the crack front of a thin elastic plate. Journal of Applied Mechanics 55, 805–813.
Newman Jr, J.C., Raju, I.S., 1983. Stress Intensity Factor Equations for Cracks in Three-dimensional Finite Bodies. ASTM Special Technical Publication STP, vol. 791, pp. 238–265.
Pook, L.P., 1994. Some implications of corner point singularities. Engineering Fracture Mechanics 48, 367–378.
Pook, L.P., 2000. Crack profiles and corner point singularities. Fatigue and Fracture of Engineering Matererials and Structures 23, 141–150.
Schnack, E., Weber, W., Zhu, Y., 2011. Discussion of experimental data for 3D crack propagation on the basis of three dimensional singularities. Computer Modeling in Engineering and Sciences 74 (1), 1–38.
Shih, C.F., Moran, B., Nakamura, T., 1986. Energy release rate along a three-dimensional crack front in a thermally stressed body. International Journal of Fracture 30, 79–102.
Sih, G.C., 1971. A review of the three-dimensional stress problem for a cracked plate. International Journal of Fracture Mechanics 7 (1), 39–61.
Zhu, W.X., 1990. Singular stress field of three-dimensional crack. Engineering Fracture Mechanics 36 (2), 239–244.